# GEOMETRIC DETERMINANTS OF CELL VIABILITY FOR 3D-PRINTED HOLLOW MICRONEEDLE ARRAY-MEDIATED DELIVERY

Sunandita Sarker<sup>1</sup>, Jinghui Wang<sup>2</sup>, Shrey A. Shah<sup>3</sup>, Christopher M. Jewell<sup>3</sup>, Kinneret Rand-Yadin<sup>4</sup>, Miroslaw Janowski<sup>2</sup>, Piotr Walczak<sup>2</sup>, Yajie Liang<sup>2</sup>, and Ryan D. Sochol<sup>1,3</sup>

<sup>1</sup>Department of Mechanical Engineering, University of Maryland, College Park, MD, USA

<sup>2</sup>Program in Image Guided Neurointerventions, Department of Diagnostic Radiology and Nuclear Medicine, University of Maryland School of Medicine, Baltimore, MD, USA

<sup>3</sup>Fischell Department of Bioengineering, University of Maryland, College Park, MD, USA

<sup>4</sup>SeeTrue Technology, LLC., Rockville, MD, USA

# **ABSTRACT**

A wide range of emerging biomedical applications and clinical interventions rely on the ability to deliver living cells via hollow, high-aspect-ratio microneedles. Recently, microneedle arrays (MNA) have gained increasing interest due to inherent benefits for drug delivery; however, studies exploring the potential to harness such advantages for cell delivery have been impeded due to the difficulties in manufacturing high-aspect-ratio MNAs suitable for delivering mammalian cells. To bypass these challenges, here we leverage and extend our previously reported hybrid additive manufacturing (or "three-dimensional printing) strategy—i.e., the combined the "Vat Photopolymerization (VPP)" technique, "Liquid Crystal Display (LCD)" 3D printing with "Two-Photon Direct Laser Writing (DLW)"—to 3D print hollow MNAs that are suitable for cell delivery investigations. Specifically, we 3D printed four sets of 650 µm-tall MNAs corresponding to needle-specific inner diameters (IDs) of 25 µm, 50 µm, 75  $\mu$ m, and 100  $\mu$ m, and then examined the effects of these MNAs on the post-delivery viability of both dendritic cells (DCs) and HEK293 cells. Experimental results revealed that the 25  $\mu$ m-ID case led to a statistically significant reduction in post-MNA-delivery cell viability for both cell types; however, MNAs with needle-specific IDs  $\geq$  50  $\mu$ m were statistically indistinguishable from one another as well as conventional 32G single needles, thereby providing an important benchmark for MNA-mediated cell delivery.

### **KEYWORDS**

Additive Manufacturing, 3D Printing, Direct Laser Writing, Microneedle Arrays, Digital Light Processing

### INTRODUCTION

Microinjection techniques for delivering cells to/into target sites via hollow microneedles are ubiquitous across research and clinical settings [1]-[4]. Traditionally, these methods have relied on singular microneedles [5]-[7]; however, given the utility of MNAs in other scenarios (e.g., drug delivery) [8]-[11], there is an uninvestigated potential for MNAs to provide similar benefits for cell delivery [12]-[14]. Previously, considerable challenges for manufacturing hollow, high-aspect-ratio MNAs at length scales relevant to cell microinjection applications have impeded efforts to explore this potential, but our recently reported VPP-DLW hybrid strategy for 3D printing such MNAs for brain microinjections offers a new pathway to enable such studies [15], [16]. Thus, here we harness and extend this hybrid MNA 3D printing strategy to provide novel means with which to investigate the influence of hollow MNAmediated delivery on acute cell viability (Fig. 1).

# MATERIALS AND METHODS

Microneedle Array (MNA) Fabrication *via* a Hybrid "Vat Photopolymerization (VPP)"-"Two-Photon Direct Laser Writing (DLW)" 3D Printing Strategy

The MNAs were fabricated by extending our previously reported hybrid 3D VPP-DLW strategy, which consists of two fundamental steps [15], [16]. First, a batch arrays of nine capillaries are 3D printed using VPP—in this case, with the Elegoo Mars 3 LCD 3D printer (Guangdong, China). Next, the MNAs are DLW-printed directly on top of each capillary using our previously reported "ex situ DLW (esDLW)" approach [15]–[17]. The computer-aided design (CAD) software, SolidWorks (Dassault Systèmes,

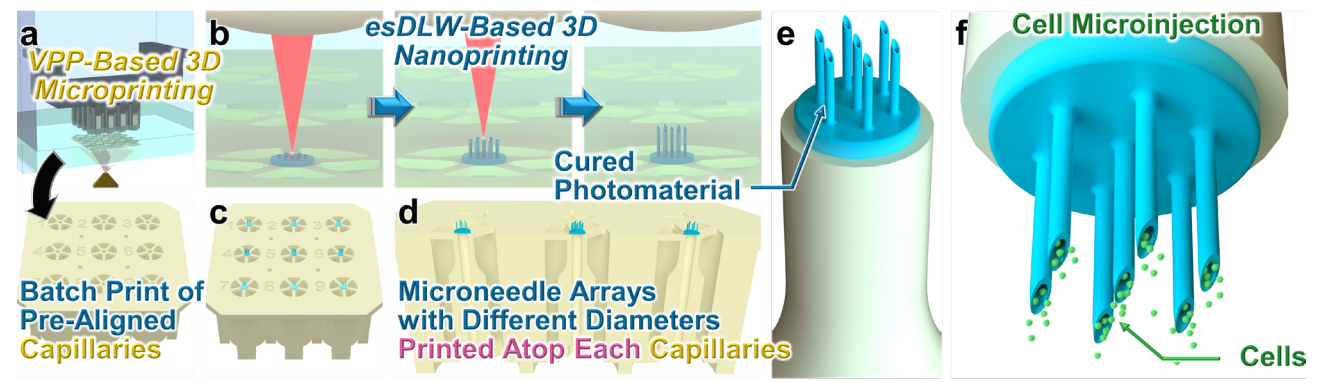


Figure 1: Microneedle array (MNA) hybrid 3D printing strategy. (a) Vat Photopolymerization (VPP)-based 3D printing of batches of pre-aligned capillaries. (b) "Ex situ Direct Laser Writing (esDLW)"-based 3D printing of MNAs directly atop each capillary. (c,d) Final (c) batch and (d) cross-sectional views of MNAs composed of microneedles with different inner diameters (IDs). (e) MNA-capillary assembly after release from the batch. (f) Cell delivery via the MNA-capillary assembly.

France), was used to generate models of batch arrays of capillaries. These capillaries were each designed with a  $650 \mu m$  ID and a 1.25 mm outer diameter (OD). The models were exported as STL files and then imported into the slicing software, Chitubox (Guangdong, China), which was used for the Elegoo Mars 3 3D printer. The capillaries were 3D printed using the Resin Clear Microfluidic v7.0a (CADworks, Canada) with a layer height set to 50  $\mu$ m. The capillaries were developed in ethanol for roughly 1 min. This step was followed by flushing ethanol through each capillary to remove any remaining resin inside. Finally, the capillaries were washed in isopropanol alcohol (IPA), dried using pressurized nitrogen gas and underwent a UV light post-curing process for 30 s to complete the preparation.

Each MNA consisted of seven needles with specific dimensions for each experimental group. These designs were saved as STL files and then processed using the computer-aided manufacturing (CAM) software DeScribe (Nanoscribe, Karlsruhe, Garmany). The printing specifications included a hatching distance of 800 nm and a layer thickness of 5  $\mu m$ . The initial step involved dispensing IP-Q photoresist (Nanoscribe) onto each capillary, after which the entire assembly was placed in the Photonic Professional GT2 3D printer (Nanoscribe, Karlsruhe, Garmany). The esDLW printing method used the Dip-in Laser Lithography (DiLL) mode, employing a 10× objective lens. The laser settings were adjusted to a power of 27.5 mW and a scanning speed of  $85,000 \mu \text{m/s}$ , with the process starting with an overlap of 75  $\mu$ m on the top surfaces of the capillaries. After completion of the esDLW printing process, the assembly was carefully removed and underwent development in propylene glycol methyl ether acetate (PGMEA) for two hours, followed by a 25-minute IPA bath. The pieces were then dried using pressurized nitrogen gas and underwent a UV light curing process for 60 seconds to complete the preparation. Finally, the targeted microneedle array-capillary was separated from the batch assembly using sharp scissors ensuring a complete detachment from the support structures (Fig. 2).

# **Optical Characterization**

All scanning electron microscope (SEM) images were

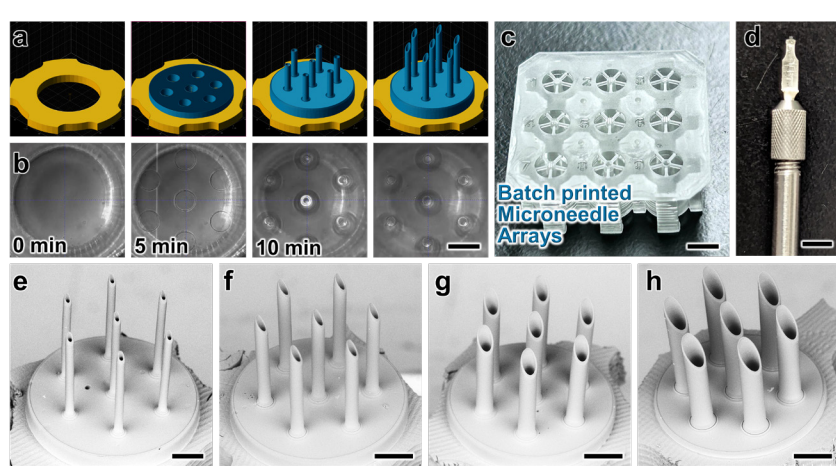


Figure 2: Fabrication results. (a, b) Simulations (a) and corresponding micrographs (b) of the esDLW process for printing an MNA atop a capillary. Scale bar = 250 µm. (c) Batch print of MNA-capillary assemblies comprising needles with different IDs. Scale bar = 5 mm. (d) MNA-capillary assembly interfaced with an adapter for fluidic loading. Scale bar = 10 mm. (e-h) SEM micrographs of MNAs comprising needlespecific IDs = (e) 25 µm, (f) 50 µm, (g) 75 µm, and (h) 100 µm. Scale bars = 250 µm.

captured using a TM4000 Tabletop SEM (Hitachi, Tokyo, Japan). Brightfield microscopy during experiments with DCss and HEK293 cells were captured using an Olympus IX-83 fluorescence microscope (Tokyo, Japan) and a Leica DMi8 automated fluorescence microscope (Wetzlar, Germany), respectively. Videography of the cell dispensing processes were conducted using Google Pixel 6 cellphone cameras.

# **Dendritic Cell (DC) Microinjection Experimentation**

Primary DCs were isolated from spleens of naïve C57BL/6 mice using CD11c+ magnetic isolation beads (Miltenyi, 130-108-338). Spleens were isolated, minced, and incubated in Spleen Dissociation Media (StemCell Technologies, 07915), dissociated using a 16G needle, passed through a 40 µm strainer, resuspended in MACS buffer containing CD11c+ magnetic isolation beads, and passed through an LS column in a magnet, with CD11c+ cells being collected in a final wash. Isolated DCs were plated at a density of 300,000 cells per 200 µL in wells of a 96-well plate. The setup for the high-throughput cell microinjection experiments is presented in Figure 3a. After aspirating and dispensing using MNAs or control needles at a controlled flow rate (O) of 1 ml/min (Fig. 3b), 10  $\mu$ l of Trypan blue was added to 10  $\mu$ l of cells, and this mixture was loaded into the hemocytometer to quantitatively measure viability. Lastly, brightfield images using a fluorescence microscope (Olympus IX-83) were used to visualize viability.

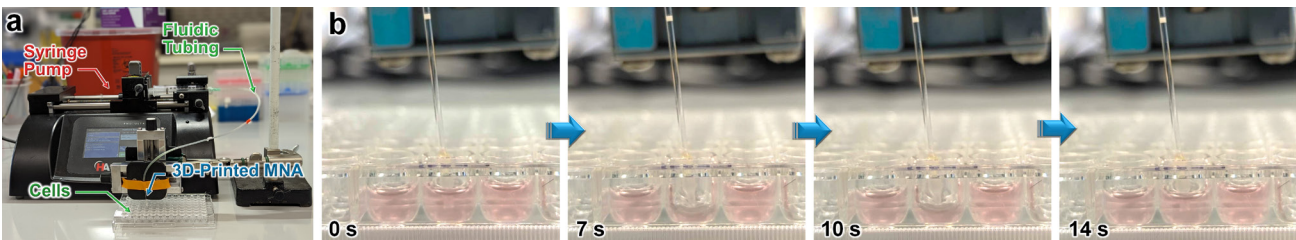


Figure 3: Dendritic cell (DC) delivery. (a) Experimental setup. (b) MNA-mediated cell aspiration and dispensing.



Figure 4: HEK293 cell delivery. (a) Experimental setup. (b, c) MNA-mediated cell (b) aspiration and (c) dispensing.

#### **HEK293 Cell Microinjection Experimentation**

The experimental setup of the HEK293 cell microinjection is presented in **Figure 4a**. HEK293 cells were seeded at a density of 25,000 cells/ $\mu$ l. Cell suspensions (20  $\mu$ l) were placed on parafilm for testing. MNAs or the control Hamilton needle were interfaced with a micromanipulator (Narishige, #MO10) and connected to a motorized pump (KD Scientific, #78-8130) for controlled delivery of cells in suspension. After aspirating 3  $\mu$ l of cells (**Fig. 4b**), 2  $\mu$ l of the aspirated cells were dispensed directly (**Fig. 4c**) in trypan blue ( $Q = 1 \mu$ l/min). This mixture was loaded into the hemocytometer to quantitatively measure cell viability and brightfield images using a fluorescence microscope (Leica DMi8) were used to visualize viability—i.e., dead cells present as blue (owing to rupture in membranes) whereas intact/live cells are not blue.

# RESULTS AND DISCUSSION Hybrid 3D Micro-Nanoprinting-Based Fabrication

The entire batch of capillaries was successfully printed using the LCD 3D printing method within 45 min (Fig. 2a). It should be noted that alternative VPP—or possibly "material jetting" 3D printing approaches [18]–[20]—could be similarly employed for fabrication of the capillary batches. The capillaries produced in this batch were designed with specific dimensions that facilitated insertion into the DLW 3D printer for esDLW-based 3D printing of different experimental groups of the MNAs. CAM simulations and corresponding micrographs of the esDLW process for 3D printing a MNA with 50 μm needle ID, directly onto a VPP-printed capillary are presented in Figure 2b and c, respectively. The esDLW printing process of different groups was completed within 15 min. SEM micrographs of fabrication results revealed a high

level of precision and alignment in fabricating the MNAs with different IDs and ODs (Fig. 2e-h).

# Cell Viability Following MNA-Meditated Delivery

In our study, we focused on understanding the effects of MNA-mediated delivery on the acute viability of cells corresponding to four distinct MNA designs that were composed of seven arrayed identical microneedles with needle-specific IDs of 25  $\mu$ m, 50  $\mu$ m, 75  $\mu$ m, or 100  $\mu$ m. The comparison involved analyzing the cell viability associated with MNAs of these varying IDs against a control group that used a conventional 32G Hamilton singular needle for cell delivery. We conducted experiments using primary splenic DCs and HEK293 cells to represent distinct microinjection scenarios. We imaged samples from each group (e.g., Fig. 5a; Fig. 6a) and then quantified the results for acute cell viability for DCs and HEK293 cells were quantified (Fig. 5b; Fig. 6b). We observed that the groups using MNAs with a 25  $\mu$ m needlespecific IDs revealed a statistically significant decrease in cell viability (p < 0.05 and p < 0.01 for the DC and HEK293 cell cases, respectively) (Fig. 5b; Fig. 6b). This decrease was evident when compared to both other MNA groups as well as the control group. In contrast, preliminary results for MNAs with needle-specific IDs of 50 µm and larger did not reveal a statistically distinguishable impact on the acute viability of both sets of cells. These results provide an important benchmark as, to our knowledge, the first demonstration that MNAs with needle-specific IDs of 50  $\mu$ m or larger could provide viable tools for cell delivery.

### **CONCLUSION**

In this work, we investigated cell microinjections through 3D-printed hollow MNAs enabled by our hybrid

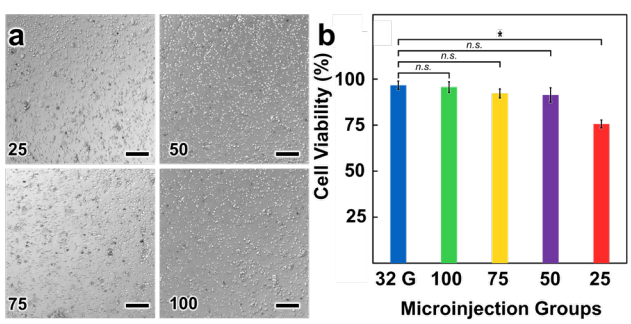


**Figure 5.** DC viability results. **(a)** Micrographs of MNA-delivered cells corresponding to each ID. Scale bars =  $100 \, \mu m$ . **(b)** Quantified results for normalized cell viability. Error bars = S.D.; n.s. = no statistical significance; \* = p < 0.05 statistical significance

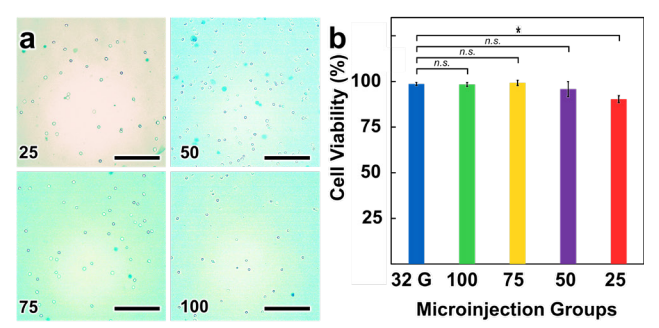


**Figure 6.** HEK293 cell viability results. **(a)** Micrographs of MNA-delivered cells corresponding to each ID. Scale bars = 250  $\mu$ m **(b)** Quantified results for normalized cell viability. Error bars = S.D.; n.s. = no statistical significance; \* = p < 0.01 statistical significance

approach that combines VPP-based 3D printing-in this case, LCD 3D printing-with esDLW-based 3D microprinting. Here we evaluated acute cell viability for both DCs and HEK293 cells delivered via MNAs with respect to needle-specific IDs of 25 µm, 50 µm, 75 µm, and 100 µm. Although the preliminary experimental results presented in this study suggest that MNAs with needlespecific IDs of 25 µm are detrimental to acute cell viability, results for MNAs with needle-specific IDs of 50 µm or larger yielded cell viability that was statistically indistinguishable from conventional 32G singular Hamilton needles. Thus, this work serves as an important first step toward potential applications in which MNAs could be harnessed for cell microinjections in both research and clinical settings, such as for stem cell therapies in the treatment of neurodegenerative conditions.

### ACKNOWLEDGEMENTS

We greatly appreciate the contributions of the members of the Bioinspired Advanced Manufacturing (BAM) Laboratory and the technical staff of Terrapin Works at the University of Maryland, College Park. This work was supported in part by U.S. National Institutes of Health (NIH) Award Numbers 1R01EB033354 and 1R41MH135827 as well as U.S. National Science Foundation (NSF) Award Number 1943356.

### CONFLICT OF INTEREST

K. Rand-Yadin is Founding Director of SeeTrue Technology, LLC., which has a potential interested in commercializing the presented MNAs. CMJ is an employee of the VA Maryland Health Care System. The views in this paper do not reflect the views of the state of Maryland or the US Government. CMJ has equity positions in Cartesian Therapeutics and Barinthus Biotherapeutics.

# REFERENCES

- [1] B. Yang, J. Kong, and X. Fang, "Programmable CRISPR-Cas9 microneedle patch for long-term capture and real-time monitoring of universal cell-free DNA," *Nat Commun*, vol. 13, no. 1, Art. no. 1, Jul. 2022.
- [2] W. Park *et al.*, "Biodegradable silicon nanoneedles for ocular drug delivery," *Science Advances*, vol. 8, no. 13, pp. eabn1772, Mar. 2022.
- [3] J. Yang *et al.*, "Recent Progress in Microneedles-Mediated Diagnosis, Therapy, and Theranostic Systems," *Advanced Healthcare Materials*, vol. 11, no. 10, pp. 2102547, 2022.
- [4] F. Pan, S. Chen, Y. Jiao, Z. Guan, A. Shakoor, and D. Sun, "Automated High-Productivity Microinjection System for Adherent Cells," *IEEE Robotics and Automation Letters*, vol. 5, no. 2, pp. 1167–1174, Apr. 2020.
- [5] S. Kusama *et al.*, "Transdermal electroosmotic flow generated by a porous microneedle array patch," *Nat Commun*, vol. 12, no. 1, Art. no. 1, Jan. 2021.
- [6] A. S. Hanafy *et al.*, "Subcellular analysis of bloodbrain barrier function by micro-impalement of vessels in acute brain slices," *Nat Commun*, vol. 14, no. 1, Art. no. 1, Jan. 2023.

- [7] L. Lin *et al.*, "Multimicrochannel Microneedle Microporation Platform for Enhanced Intracellular Drug Delivery," *Advanced Functional Materials*, vol. 32, no. 21, pp. 2109187, 2022.
- [8] S. A. Shah, R. S. Oakes, S. M. Kapnick, and C. M. Jewell, "Mapping the Mechanical and Immunological Profiles of Polymeric Microneedles to Enable Vaccine and Immunotherapy Applications," Frontiers in Immunology, vol. 13, 2022.
- [9] C. Edwards, Shrey. A. Shah, T. Gebhardt, and C. M. Jewell, "Exploiting Unique Features of Microneedles to Modulate Immunity," *Advanced Materials*, vol., pp. 2302410, Nov 2023.
- [10] Z. Chen et al., "3D-Printed Integrated Ultrasonic Microneedle Array for Rapid Transdermal Drug Delivery," Mol. Pharmaceutics, vol. 19, no. 9, pp. 3314–3322, Aug. 2022.
- [11] M. Dervisevic *et al.*, "Transdermal Electrochemical Monitoring of Glucose via High-Density Silicon Microneedle Array Patch," *Advanced Functional Materials*, vol. 32, no. 3, pp. 2009850, 2022.
- [12] Y. Han, J. Li, T. Chen, B. Gao, and H. Wang, "Modern microelectronics and microfluidics on microneedles," *Analyst*, vol. 148, no. 19, pp. 4591–4615, 2023.
- [13] C. Vissers, G.-L. Ming, and H. Song, "Nanoparticle technology and stem cell therapy team up against neurodegenerative disorders," *Adv Drug Deliv Rev*, vol. 148, pp. 239–251, Aug. 2019.
- [14] A. S. Lee *et al.*, "Prolonged survival of transplanted stem cells after ischaemic injury via the slow release of pro-survival peptides from a collagen matrix," *Nat Biomed Eng*, vol. 2, no. 2, Art. no. 2, Feb. 2018.
- [15] S. Sarker *et al.*, "3D-Printed Microinjection Needle Arrays via a Hybrid DLP-Direct Laser Writing Strategy," *Advanced Materials Technologies*, vol. 8, no. 5, pp. 2201641, 2023.
- [16] S. Sarker *et al.*, "A Hybrid 3D Micro-Nanoprinting Approach for Biomedical Microinjection Needle Arrays," in the proceedings of Hilton Head Workshop 2022: A Solid-State Sensors, Actuators and Microsystems Workshop, Jun. 5-9 2022, pp. 27–30
- [17] R. Acevedo *et al.*, "3d Nanoprinted External Microfluidic Structures Via Ex Situ Direct Laser Writing," in 2021 IEEE 34th International Conference on Micro Electro Mechanical Systems (MEMS), Jan. 2021, pp. 10–13.
- [18] R. D. Sochol *et al.*, "3D printed microfluidic circuitry via multijet-based additive manufacturing," *Lab Chip*, vol. 16, no. 4, pp. 668–678, Feb. 2016.
- [19] J. D. Hubbard *et al.*, "Fully 3D-printed soft robots with integrated fluidic circuitry," *Science Advances*, vol. 7, no. 29, pp. eabe5257, Jul. 2021.
- [20] B. Hayes, T. Hainsworth, and R. MacCurdy, "Liquid–solid co-printing of multi-material 3D fluidic devices via material jetting," *Additive Manufacturing*, vol. 55, pp. 102785, Jul. 2022.

### **CONTACT**

\*S.Sarker, tel: +1-301-405-6928; ssarker1@umd.edu